Sensors and Materials, Vol. 30, No. 7 (2018) 1547–1554
MYU Tokyo

S & M 1610

Characterizations of Ce-doped $Y_4Al_2O_9$ Crystals for Scintillator Applications

Go Okada,[1*] Masaki Akatsuka,[1] Hiromi Kimura,[1] Masaki Mori,[2†]
Naoki Kawano,[1] Noriaki Kawaguchi,[1] and Takayuki Yanagida[1]

[1]Graduate School of Materials Science, Nara Institute of Science and Technology (NAIST),
8916-5 Takayama, Ikoma, Nara 630-0192, Japan
[2]Yamazaki Manufacturing Department, Hitachi Metals Ltd.
15-17 2 Chome, Egawa, Shimamoto Mishima, Osaka 618-0013, Japan

(Received December 19, 2017; accepted April 11, 2018)

Keywords: scintillator, $Y_4Al_2O_9$, YAM, Ce^{3+}

Ce-doped $Y_4Al_2O_9$ (YAM) crystals were grown by the floating zone method, and several different characterizations were conducted for scintillator applications. Both photoluminescence (PL) and scintillation show emissions predominantly due to the 5d–4f transitions of Ce^{3+} over 400–600 nm. The luminescence lifetime is approximately 10 ns for PL while the scintillation decay curve is best fitted by a second-order exponential decay function with the lifetimes of approximately 30 and 300 ns. These lifetimes are faster than that for Ce:$Y_3Al_5O_{12}$ (YAG) (~120 ns) and close to that of Ce:$YAlO_3$ (YAP) (~30 ns). The Ce-doped YAM shows a relatively high afterglow signal induced by X-rays (2 ms pulse) possibly due to the inclusion of a large number of defect centers. Pulse height spectroscopy was demonstrated under alpha-ray irradiation, and a successful sample showed a full-energy peak.

1. Introduction

Inorganic phosphors are often a tool for radiation measurement applications.[(1)] Such devices are commonly referred to as scintillators and storage phosphors depending on the phenomenon involved. The scintillators convert the incident radiation energy to light immediately so that one can detect radiation signals using conventional photodetectors on-line. The storage phosphors, on the other hand, store and accumulate the incident radiation energy for a certain period of time until read-out. The stored signal is then read out as light emission stimulated by heat or light, in which the light emission intensity is proportional to the stored energy, hence the stored radiation dose. Both scintillators and storage phosphors involve different mechanisms; however, they are considered to undergo some common processes. First, upon interactions of incident radiation with matter, in both scintillators and dosimeters, electrons and holes are generated. In scintillators, next, the generated charges transfer to luminescent centers and recombine to emit light, while in storage phosphors, the charges are captured by trapping centers and stored.

*Corresponding author: e-mail: go-okada@ms.naist.jp
†Former student of NAIST and currently at Hitachi Metals Ltd.
http://dx.doi.org/10.18494/SAM.2018.1919

By applying external heat or light, the captured charges are ionized and then recombine at luminescent centers to emit light, as in scintillators. When the stimulant is heat, the resultant luminescence is so-called thermally stimulated luminescence (TSL),[2] while the luminescence generated by light stimulation is the so-called optically stimulated luminescence (OSL).[3,4] With knowledge of the luminescence processes above, it is clear that the luminescence efficiencies of scintillators and storage phosphors conflict.[5–8] Those phosphor materials are used in a wide range of application fields such as medicine,[9] security,[10] high-energy physics,[11] and geophysical and resource explorations.[12] The required properties depend on the application so there are many different scintillator materials available, but no scintillators satisfy the requirements of all the applications. In addition, the application technologies continue to advance and require sensing materials with better properties. Therefore, a search for new materials is continuously demanded.

Yttrium aluminum monoclinic (YAM) crystals are our current interest. The YAM is one in the Y_2O_3–Al_2O_3 compound group after yttrium aluminum garnet (YAG) and yttrium aluminum perovskite (YAP). It can be expressed by the formula $Y_4Al_2O_9$ and has the space group P21/c with a monoclinic crystal structure.[13,14] The yttrium site can be substituted by, for example, a series of rare-earth ions to act as a luminescence center while the Al site can be substituted by Ga and some transitional metals. These features are similar to those of the garnet and perovskite groups. The luminescence properties, including scintillation and storage-luminescence properties, of garnets and perovskites have been intensively studied with many different combinations of these constituent elements.[15–20] Despite the similarities to the garnets and perovskites, fewer studies have been reported on the luminescence properties of the monoclinic crystals. As far as we are aware, the scintillation properties of Ce-doped YAM (Ce:YAM) have not been reported, and only a few groups have investigated some optical properties including photoluminescence.[21,22]

This contribution is a comprehensive report on the optical properties of Ce:YAM crystals for scintillator applications. We have synthesized the Ce:YAM crystals with different concentrations of Ce^{3+} from 0.3 to 1 mol% by the floating zone (FZ) method. Furthermore, we have investigated the photoluminescence (PL) spectrum, PL quantum yield (QY), PL lifetime, scintillation spectrum/lifetime, afterglow, and pulse height spectroscopic properties.

2. Materials and Methods

Ce:YAM single crystals with different concentrations of Ce from 0.3 to 1 mol.% were synthesized by the FZ method. The raw powders of Y_2O_3, Al_2O_3, and CeO_2 of reagent grade (4N purity) were homogeneously mixed in stoichiometric compositions. Here, the Ce ion was introduced to the host constitution as $(Y_{1-x}Ce_x)_4Al_2O_9$ (x = 0.003, 0.005, 0.008, and 0.010). The mixed powder of each composition was formed into a cylindrical rod (ø4 mm × 50 mm) by applying hydrostatic pressure inside a pencil balloon and then sintered at 1500 °C for 6 h in air to obtain a solid ceramic rod. Crystal growth was accomplished by the FZ method using an FZ furnace (FZD0192, Canon Machinery) in air. A pair of ceramic rods was placed at the center of the mirror furnace equipped with two halogen lamps. The infrared light from the lamps

was focused on adjacent ends of the ceramic rods to cause melting, and the rods were rotated in alternating directions to each other at a rate of 20 rpm. The set of ceramic rods was slowly translated vertically at 5–6 mm/h to slowly cool the melt and obtain a crystal.

PL emission and excitation spectra were measured using a spectrofluorometer (FP8600, JASCO). The PL decay curve was measured using Quantaurus-τ (C11367, Hamamatsu Photonics) to obtain the lifetime. The lifetime was extracted from the measured decay curve by least-squares fitting with a sum of two or three exponential decay functions. The system offers a time resolution of 60 ps.

Scintillation spectra were measured using a laboratory-constructed setup. Detailed descriptions can be found elsewhere;[19] but briefly, a CCD-based spectrometer (DU920-BU2NC, ANDOR) was used to measure a scintillation spectrum while the sample was irradiated by X-rays generated by a conventional X-ray tube (40 kV and 5.2 mA; W anode; Be window). The scintillation photons were guided to the spectrometer through an optical fiber.

The X-ray-induced scintillation decay time and afterglow profiles were measured using a characterization system equipped with a pulse X-ray source. The details of system descriptions can be found elsewhere.[23] The system is available as a custom-ordered product from Hamamatsu Photonics. The system offers a time resolution of a few ns, and a decay curve profile was collected on the basis of a time-correlated single photon counting (TCSPC). The voltage applied to the X-ray tube was 30 kV.

Pulse height spectroscopy measurements were performed in order to demonstrate the capability of being used in a scintillation counter and to test the light yield, which is the number of emission photons per incident radiation quantum. A sample was placed on the window of the photomultiplier tube (PMT; R7600, Hamamatsu Photonics) with optical coupling grease (OKEN6262A), and the sample was covered by several layers of Teflon reflectors. A power supply (ORTEC556) was used to apply a bias voltage of −700 V to the PMT. The output electrical signal from the PMT was sent to a preamplifier (ORTEC 113) and then a shaping amplifier (ORTEC 572) with a 0.5 μs shaping time. Furthermore, the signal was processed by a multichannel analyzer (Pocket MCA 8000A, Amptek) to convert analog signals to digital, and the pulse height spectrum was constructed on the computer. We used sealed radioactive ^{241}Am α-ray (5.5 MeV) and ^{137}Cs γ-ray (662 keV) sources in the measurements.

3. Results and Discussion

Figure 1 illustrates the synthesized YAM crystals with different concentrations of Ce. The typical size of the obtained crystal rods was ~4 mm in diameter and ~50 mm in length. The obtained crystal rods were cut into small pieces for characterization. The obtained crystals appear milky, the degree of which seems to increase with increasing dopant concentration. The cause can be inclusions of cracks and possibly secondary phases [although no secondary phase was detected by X-ray diffraction (XRD)]. Figure 2 shows the XRD patterns of the YAM crystals synthesized. All the samples showed the monoclinic structure with the pattern consistent with that in an earlier study.[24] The dominant crystal phase is monoclinic.

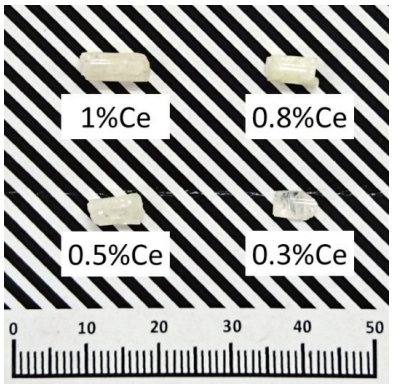

Fig. 1. (Color online) Synthesized YAM crystals doped with various concentrations of Ce.

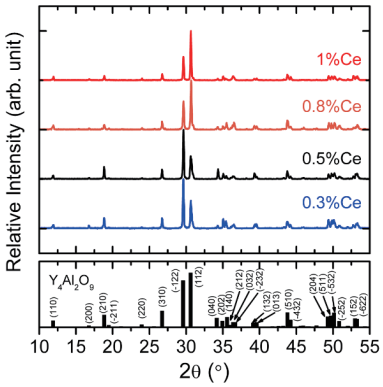

Fig. 2. (Color online) Powder XRD patterns of obtained crystals with different concentrations of Ce. A reference pattern of $Y_4Al_2O_9$ crystal is also given at the bottom.[24]

The PL excitation and emission spectra are illustrated in Fig. 3. When excited at 280 nm, a broad emission was observed from 400 to 600 nm. The latter emission has a weak excitation band around 360 nm and a strong band below 300 nm. The origins of the emission and excitation bands were ascribed to the $5d_1 \rightarrow 4f$ transitions (emission) and $4f \rightarrow 5d_1$ transitions (excitation) of the Ce^{3+} ion. A strong absorption band below 300 nm is most likely due to the $4f \rightarrow 5d_2$ transitions of Ce^{3+} as well as absorption by the Ce^{4+} ion. The PL quantum yields were too low to measure, i.e., less than ~3%.

Figure 4 shows the PL decay profiles. The excitation and emission wavelengths were fixed at 365 and 480 nm for all samples. The obtained curves were best-fitted with a sum of two exponential decay functions to determine the lifetimes. The lifetimes (and relative intensities) obtained are: 2.4 ns (90%) and 10 ns (10%) for 0.3%, 2.1 ns (85%) and 11 ns (15%) for 0.5%, 2.2 ns (89%) and 9.6 ns (11%) for 0.8%, and 2.0 ns (83%) and 9.9 (17%) ns for 1% Ce-doped samples. The shorter values for each set of lifetimes are considered to be the instrumental response, and the longer values of approximately 10 ns are the PL lifetimes due to the 5d–4f transitions of Ce^{3+}. These values are the fastest among the Ce-doped Y_2O_3–Al_2O_3 compounds (~30 ns for Ce:$YAlO_3$[25] and ~120 ns for Ce:$Y_3Al_5O_{12}$[26]). The correlation with the dopant concentration is not significant, but the lifetime seems to decrease with the concentration, possibly due to increasing nonradiative relaxation processes upon concentration quenching. It is worth mentioning that an earlier study[21] reported that the lifetime of PL is on the order of a few ns. Some possible explanations of the difference from the results of our study are that (1) the reported emission component is hidden in the instrumental response in our measurements, and (2) the slower signal was not detected in the earlier report because the measurement time range was short (~10 ns).

The X-ray-induced scintillation spectra are demonstrated in Fig. 5. As observed for PL (Fig. 3), the scintillation spectrum consists of a broad band over 400–600 nm. For the similarities in the spectral features with those of PL, it is straightforward that the emission origin can be attributed to the 5d–4f transitions of Ce^{3+}. As indicated in the figure, the peak position seems to red-

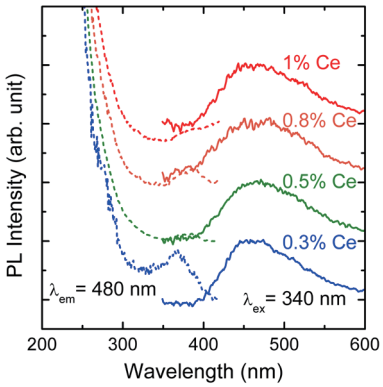

Fig. 3. (Color online) PL excitation and emission spectra of YAM samples doped with Ce.

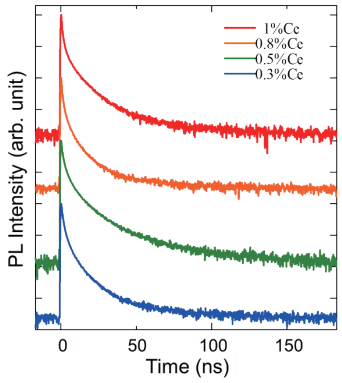

Fig. 4. (Color online) PL decay profiles of Ce:YAM. The excitation wavelength is 365 nm while the emission wavelength monitored is 480 nm.

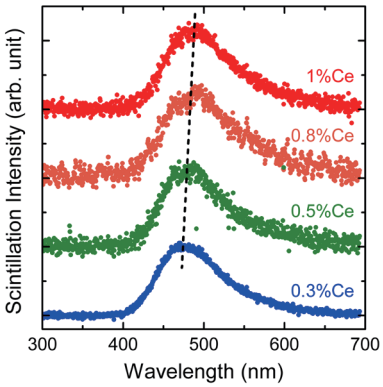

Fig. 5. (Color online) X-ray-induced scintillation spectra of Ce:YAM crystals. The X-ray irradiation was performed by using a conventional X-ray tube (80 keV, W anode, Be window).

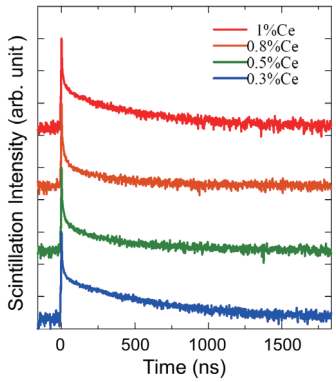

Fig. 6. (Color online) X-ray-induced scintillation decay curves of Ce:YAM crystals. The X-ray irradiation was performed by using a pulse X-ray tube (30 keV, W anode, Be window).

shift with increasing concentration of Ce. This is typically seen in many Ce-doped materials because of self-absorption in which a fraction of emission is absorbed by the material itself as it travels in the matrix. It should be noted that a clear redshift was not apparent in PL owing to the difference in the measurement geometry. The PL was measured on the same sample surface of excitation while the scintillation photon was collected to be measured on the opposite side from the irradiation source so the self-absorption is more strongly affected. Despite the effect of self-absorption, the emission wavelength seems to be shorter than that of YAG:Ce and longer than that of YAP:Ce where the peak positions are 540 and 360 nm, respectively.

Figure 6 shows scintillation decay curves of Ce:YAM crystal samples induced by pulse X-rays. All the decay curves are best approximated by a third-order exponential decay function. The deducted lifetimes (and relative intensities) are: 1.9 ns (80%), 37 ns (14%), and 400 ns (6%) for 0.3%, 6.4 ns (90%), 38 ns (4%), and 240 ns (6%) for 0.5%, 5.6 ns (90%), 28 ns (6%), and 250 ns (4%) for 0.8%, and 1.6 ns (80%), 25 ns (15%), and 320 ns (5%) for 1% Ce-

doped samples. The shortest lifetimes detected for all the samples are due to the instrumental response. The intermediate values are of a similar order to those observed in PL for the 5d–4f transitions of Ce^{3+}, so we attribute the same origins. The origins of the longest contributions are unknown and further investigations are needed to identify them; however, a possibility is that some types of defects act as luminescent centers. No luminescence features are observed in the scintillation spectrum other than that for Ce^{3+} (Fig. 5); thus, most likely, the luminescence of this slowest component is located in the same spectral range and overlapped with the emission of Ce^{3+}. These lifetimes are found to be longer than that of PL. An explanation for this is that the processes of excitation and radiative relaxation at only the localized luminescent center are observed by PL whereas the energy transfer process from the host matrix to the luminescent center must also be taken into account. Thus, it appears to decay slower in scintillation. Furthermore, compared with Ce-doped YAG (Ce:YAG) and Ce-doped YAP (Ce:YAP) crystals, the intermediate luminescence due to Ce^{3+} in Ce:YAM is considerably shorter than that of Ce:YAG (~120 ns) and equivalent to that of Ce:YAP (~30 ns).

The X-ray-induced afterglow profiles of Ce:YAM crystal samples are shown in Fig. 7. Here, the afterglow level is defined as the percentage of intensity at 20 ms after a pulse irradiation relative to the intensity during irradiation. The afterglow levels of the 0.3, 0.5, 0.8, and 1.0% Ce-doped samples are 0.05, 0.07, 0.03, and 0.05%, respectively. Compared with common X-ray scintillators (e.g., $Bi_4Ge_3O_{12}$, $CdWO_4$, and Tb and Pr co-doped Gd_2O_2S),[23] those afterglow levels are still considerably higher as common scintillators have afterglows of ~10 ppm at several milliseconds after irradiation.

Pulse height spectroscopy was demonstrated using the Ce:YAM crystal samples with 5.5 MeV α-ray irradiation of ^{241}Am, and the obtained spectra are illustrated in Fig. 8. Among the samples tested, only the 0.3% Ce-doped sample showed a full-energy peak. We think this is because, on the basis of the visual appearance, the crystal quality of this sample is the best, and scintillation light is effectively detected by the PMT without scattering loss. Therefore, better performance is expected for the other samples by improving the crystal quality. In addition, the

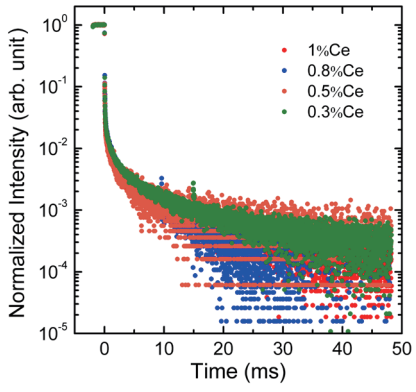

Fig. 7. (Color online) X-ray-induced afterglow profiles. The X-ray source was a pulse X-ray tube (30 keV, W anode, Be window), and the irradiation pulse width was 2 ms.

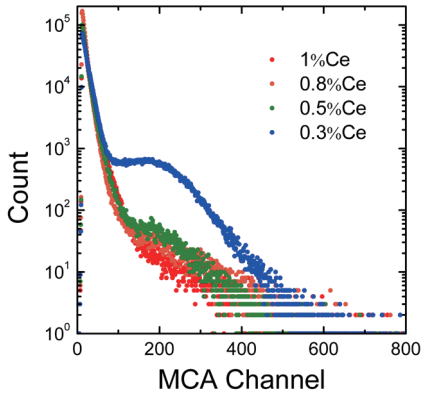

Fig. 8. (Color online) Pulse height spectra of 5.5 MeV α-rays of ^{241}Am measured using the Ce:YAM crystal samples.

YAM structure has four different Y sites in a unit cell (substituted by Ce^{3+} ions), which could cause concentration quenching of luminescence by the Ce^{3+} ion.[27] We also examined pulse height spectroscopy under ^{137}Cs γ-ray irradiation, but the light yield was so small that a full-energy peak was not observed even with the 0.3% Ce-doped sample.

4. Conclusions

Ce:YAM crystals were synthesized by the FZ technique and the optical properties were studied for scintillator applications. For both PL and scintillation, a broad emission band is observed over 400–600 nm owing to the 5d–4f transitions of the Ce^{3+} ion. The spectral position is, in fact, shorter than that of Ce:YAG (540 nm) and longer than that of Ce:YAP (360 nm). The peak position seems to slightly redshift with increasing concentration of Ce^{3+} owing to self-absorption. Despite the similarity in the spectral features between PL and scintillation, the decay time constants are notably different. The PL decay constants are ~10 nm and almost independent of the concentration of Ce, whereas the scintillation decay times are much longer (~30 and 200–300 ns). In addition, the scintillation decay time slightly decreased with increasing concentration of Ce, most likely due to the concentration quenching effect. Compared with Ce:YAG (~120 ns), the scintillation decay time is much shorter but equivalent to that of Ce:YAP (~30 ns). The X-ray-induced afterglow level is on the order of 10^{-2}, which is considerably larger than those of commercial scintillators (ppm). A pulse height spectrum of α-rays (^{241}Am) using Ce:YAM shows a clear full-energy peak, but the light yield and crystalline quality are insufficient for a clear peak to be observed under γ-rays. Further efforts must be made to enhance the scintillation properties before Ce:YAM crystals can be considered for a practical scintillator.

Acknowledgments

This work was supported by Grant-in-Aid for Scientific Research (A) (17H01375), Grant-in-Aid for Young Scientists (B) (17K14911), and Grant-in-Aid for Research Activity Start-up (16H06983) from the Ministry of Education, Culture, Sports, Science and Technology of the Japanese government (MEXT), as well as A-STEP from the Japan Science and Technology Agency (JST). The Cooperative Research Project of the Research Institute of Electronics, Shizuoka University, Mazda Foundation, Konica Minolta Science and Technology Foundation, NAIST Foundation, and TEPCO Memorial Foundation are also acknowledged.

References

1 G. F. Knoll: Radiation Detection and Measurement (Wiley, Denvers, 2010) 4th ed.
2 S. W. S. McKeever: Thermoluminescence of Solids (Cambridge University Press, Cambridge, 1985).
3 H. Nanto, A. Nishimura, M. Kuroda, Y. Takei, Y. Nakano, T. Shoji, T. Yanagita, and S. Kasai: Nucl. Instrum. Methods Phys. Res., Sect. A **580** (2007) 278.
4 H. von Seggern: Braz. J. Phys. **29** (1999) 254.
5 T. Yanagida, Y. Fujimoto, K. Watanabe, N. Kawaguchi, K. Fukuda, Y. Miyamoto, and H. Nanto: 2013 IEEE Nuclear Science Symp. and Medical Imaging Conf. (2013) 1.

6 T. Yanagida, Y. Fujimoto, K. Watanabe, K. Fukuda, N. Kawaguchi, Y. Miyamoto, and H. Nanto: Radiat. Meas. **71** (2014) 162.
7 T. Yanagida: J. Lumin. **169** (2016) 544.
8 G. Okada, K. Fukuda, N. Kawaguchi, and T. Yanagida: Radiat. Meas. **106** (2017) 134.
9 T. Yanagida, A. Yoshikawa, Y. Yokota, K. Kamada, Y. Usuki, S. Yamamoto, M. Miyake, M. Baba, K. Kumagai, K. Sasaki, M. Ito, N. Abe, Y. Fujimoto, S. Maeo, Y. Furuya, H. Tanaka, A. Fukabori, T. Rodrigues dos Santos, M. Takeda, and N. Ohuchi: IEEE Trans. Nucl. Sci. **57** (2010) 1492.
10 D. Totsuka, T. Yanagida, K. Fukuda, N. Kawaguchi, Y. Fujimoto, J. Pejchal, Y. Yokota, and A. Yoshikawa: Nucl. Instrum. Methods Phys. Res., Sect. A **659** (2011) 399.
11 K. Yamaoka, M. Ohno, Y. Terada, S. Hong, J. Kotoku, Y. Okada, A. Tsutsui, Y. Endo, K. Abe, Y. Fukazawa, S. Hirakuri, T. Hiruta, K. Itoh, T. Itoh, T. Kamae, M. Kawaharada, N. Kawano, K. Kawashima, T. Kishishita, T. Kitaguchi, M. Kokubun, G. M. Madejski, K. Makishima, T. Mitani, R. Miyawaki, T. Murakami, M. M. Murashima, K. Nakazawa, H. Niko, M. Nomachi, K. Oonuki, G. Sato, M. Suzuki, H. Takahashi, I. Takahashi, T. Takahashi, S. Takeda, K. Tamura, T. Tanaka, M. Tashiro, S. Watanabe, T. Yanagida, and D. Yonetoku: IEEE Trans. Nucl. Sci. **52** (2005) 2765.
12 T. Yanagida, Y. Fujimoto, S. Kurosawa, K. Kamada, H. Takahashi, Y. Fukazawa, M. Nikl, and V. Chani: Jpn. J. Appl. Phys. **52** (2013) 76401.
13 H. Yamane, M. Shimada, and B. A. Hunter: J. Solid State Chem. **141** (1998) 466.
14 H. Yamane, T. Nagasawa, Y. Murakami, T. Kamata, D. Shindo, M. Shimada, and T. Endo: Mater. Res. Bull. **33** (1998) 845.
15 M. Mori, G. Okada, N. Kawaguchi, and T. Yanagida: Jpn. J. Appl. Phys. **56** (2017) 12603.
16 T. Yanagida, Y. Fujimoto, H. Yagi, T. Yanagitani, M. Sugiyama, A. Yamaji, and M. Nikl: Opt. Mater. **35** (2013) 788.
17 T. Oya, G. Okada, and T. Yanagida: J. Ceram. Soc. Jpn. **124** (2016) 536.
18 T. Kuro, D. Nakauchi, G. Okada, N. Kawaguchi, and T. Yanagida: Opt. Mater. **64** (2017) 282.
19 T. Yanagida, K. Kamada, Y. Fujimoto, H. Yagi, and T. Yanagitani: Opt. Mater. **35** (2013) 2480.
20 T. Yanagida, Y. Fujimoto, M. Koshimizu, K. Watanabe, H. Sato, H. Yagi, and T. Yanagitani: Opt. Mater. **36** (2014) 2016.
21 B. Fetlinski, Z. Boruc, M. Kaczkan, S. Turczynski, D. Pawlak, and M. Malinowski: J. Lumin. **181** (2017) 133.
22 H.-W. Wei, X.-M. Wang, X.-J. Kuang, C.-H. Wang, H. Jiao, and X.-P. Jing: J. Mater. Chem. C **5** (2017) 4654.
23 T. Yanagida, Y. Fujimoto, T. Ito, K. Uchiyama, and K. Mori: Appl. Phys. Express **7** (2014) 62401.
24 X. Zhan, Z. Li, B. Liu, J. Wang, Y. Zhou, and Z. Hu: J. Am. Ceram. Soc. **95** (2012) 1429.
25 J. A. Mares, M. Nikl, N. Solovieva, C. D'Ambrosio, F. De Notaristefani, K. Blazek, P. Maly, K. Nejezchleb, P. Fabeni, G. P. Pazzi, J. T. M. De Haas, C. W. E. Van Eijk, and P. Dorenbos: Nucl. Instrum. Methods Phys. Res., Sect. A **498** (2003) 312.
26 E. Mihóková, M. Nikl, J. A. Mareš, A. Beitlerová, A. Vedda, K. Nejezchleb, K. Blažek, and C. D'Ambrosio: J. Lumin. **126** (2007) 77.
27 W. Y. Ching and Y. Xu: Phys. Rev. B **59** (1999) 12815.